Constitutive modeling of strain-induced crystallization in filled rubbers

Roozbeh Dargazany,[1,2] Vu Ngoc Khiêm,[1] Emad A. Poshtan,[1] and Mikhail Itskov[1]
[1]*Department of Continuum Mechanics, RWTH Aachen University, 52062 Aachen, Germany*
[2]*Department of Civil and Environmental Engineering, Michigan State University, East Lansing, MI 48824, USA*
(Received 6 November 2013; published 25 February 2014)

Strain-induced crystallization is a unique crystallization process taking place solely in polymers subjected to large deformations. It plays a major role for reinforcement and improvement of mechanical properties of polymers with a high regularity of the molecular structure. In this paper, we develop a micromechanical model for the strain-induced crystallization in filled rubbers. Accordingly, the strain-induced crystallization is considered as a process triggered by fully stretched and continued by semistretched polymer chains. The model extends the previously proposed network evolution model [Dargazany and Itskov, Int. J. Solids Struct. **46**, 2967 (2009)] and can thus, in addition to the stress upturn and evolution of crystallinity, take into account several inelastic features of filled rubbers, such as the Mullins effect, permanent set, and induced anisotropy. Finally, the accuracy of the model is verified against different set of experimental data both with respect to the stress-strain and crystallization-strain relations. The model exhibits good agreement with the experimental results, which, besides its relative simplicity, makes it a good option for finite-element implementations.

DOI: 10.1103/PhysRevE.89.022604 PACS number(s): 61.41.+e, 64.70.dg, 62.20.F−, 46.15.−x

I. INTRODUCTION

Crystallization is an important type of reinforcement used in various natural and industrial materials, such as spider silk, moth silk, rubbers, and so on.

In polymers, the crystallization process can be triggered by applied deformation, reduction of the melt temperature, or evaporation of the solvent. Deformation- or strain-induced crystallization (SIC) takes place only in certain polymers that possess regular and oriented polymer chains as, for example, polybutadiene (BR), butyl (IIR), polyisoprene (IR), polychloroprene (CR), and natural rubber (NR).

Generally, one can consider two important aspects in understanding SIC. The first one is the crystalline morphology which explains the mechanism of crystalline formation. The second one is a constitutive model which proposes concepts for the stress upturn and stress softening observed in cyclic loading of NR undergoing SIC.

In the past few decades, the morphology of crystals formed by SIC has been extensively studied, and its different features have been investigated experimentally and described by several theories, which can be categorized into the three groups itemized below.

Fringed-micelle: This was one of the earliest models developed to describe the morphology of crystals in a semicrystallized rubber matrix [1]. The model considers crystals as a compact alignment of different polymer chains at certain points. Thereby, a polymer chain takes part in several crystallites (Fig. 1). The model explains the existence of fibrillar crystallites and predicts their growth direction normal to the chain axis.

Folded chain model: In contrast to the fringed micelle model, early electron diffraction observations [2,3] suggest the formation of thin lamella-like plates of polymers normal to the stretch direction. To describe these plates, the folded chain model was developed.

The first generation of the folded chain models were based on the adjacent re-entry concept [4], where chains are assumed to come back and forth into one lamella and form loops with identical lengths [Fig. 2(a)]. Thus, the resultant lamella has a clear cuboid shape which was later used to explain the existence of the spherulite structures.

Shortly afterwards, Flory [5] demonstrated that the adjacent re-entry model cannot precisely describe the crystal formation in long chain molecules. He showed mathematically that a significant amount of chains do not return to the lamella after departure from it. Thus, an irregular re-entry model based on variable lengths of chain loops in the lamella [see Fig. 2(b)] was proposed. It is also possible that some chains do not re-enter the same lamella but rather join other ones. These chains may eventually come back to the amorphous region. This conformation of chain folding is often referred to as the switchboard model, since the irregular entrance and exit of chains from the lamella surface makes the lamella look like old switchboards.

The switchboard model can also be applied to explain the crystallization from the melt in polymers [6,7]. The model also confirms the existence of multilayer crystals and loose end chains which were found by small-angle neutron scattering experiments of melt-crystallized polymers [8,9].

Extended chain model: This is an extension of the folded chain model aimed to further take the formation of fibrillar crystals into account. The model considers fibrillar crystals as nuclei around which the spherulites are formed. Thus, the final crystal, generally referred to as a shish-kebab structure, is a combination of both fibrillar and lamellar crystals (see Fig. 3). Accordingly, the model considers a two-step nucleation and growth procedure. The first step is associated with the formation of fibrillar crystals (shish) from extended polymers while the second one includes the formation of spherulites around the fibrillar crystals.

In spite of this progress in crystalline morphology, the modeling of SIC still remains somewhat restricted. Most studies on the polymer crystallization focus on the temperature-induced crystallization rather than on the strain-induced one [10,11].

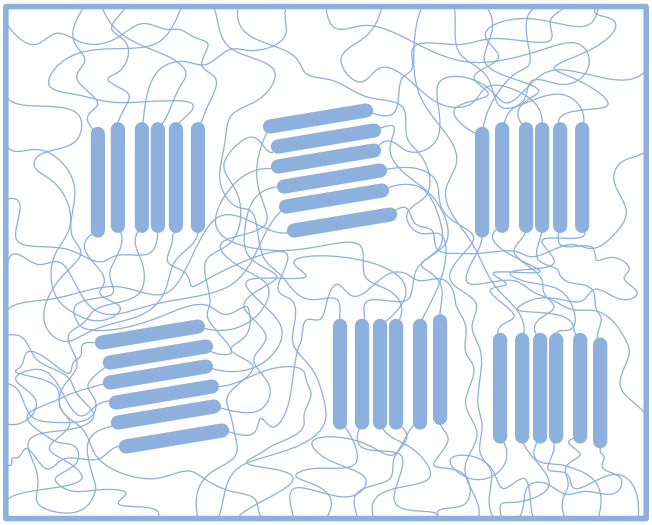

FIG. 1. (Color online) Illustration of the fringed micelle model.

Early approaches to the modeling of SIC were focused mostly on the thermodynamic formulation of crystallization [12,13]. Thus, Flory proposed that the degree of crystallization can be expressed in terms of the change in the melting point T_m, which in turn is a function of the stretch ratio. On the basis of the deformation calorimetry, Göritz and Müller [14,15] showed that this relation between the degree of crystallization and elongation [12] is applicable only for crystallization in the extended state of polymer chains.

Considering crystallines to be mainly of the lamellar type, Saidan [16] developed an isotropic model where the semicrystallized network acts in series with the amorphous region. On the contrary, other models considered the crystallized and amorphous networks to operate parallel to each other. Their individual contributions were formulated by a phenomenological law [17,18].

Flory [12,19] suggested that induced crystallites can be regarded as a source of reinforcement in rubbers. Following this idea, Rault *et al*. [20] assumed a two-network system where crystallites play a role of highly functional cross-links.

Fukahori [21] elaborated another mechanism for the strain-induced crystallization in natural rubber. Accordingly, crystals are formed by un-cross-linked polymer chains which further act as linkages in the rubber network and lead to the stress upturn at large extensions.

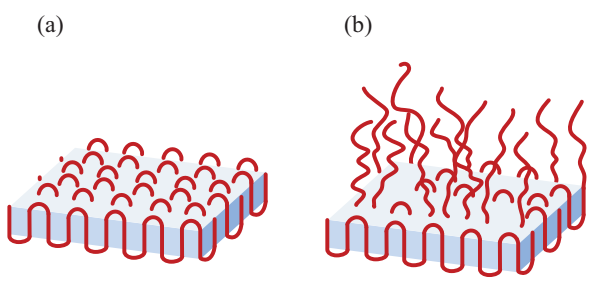

FIG. 2. (Color online) A schematic view of a lamella in the (a) adjacent re-entry and (b) switchboard models.

Toki *et al*. [22–24] proposed to decompose the rubber matrix after SIC into three phases: (i) an unoriented amorphous phase, (ii) an oriented amorphous phase, and (iii) a crystalline phase. Expanding this idea, Tosaka *et al*. [25] developed a micromechanical concept that considers existence of different chain lengths between two constraints (aggregates or cross-links). Accordingly, under tension the shorter chains become fully stretched and subsequently form nucleation sites for crystallites.

Kroon [26] further developed this idea by implementing it into a full network model which takes the anisotropic crystal nucleation of the unfilled rubber into account. The model is based on an empirical approach and is able to predict both the stress-stretch hysteresis and the evolution of the crystallization degree under deformation.

Recently, Zhang *et al*. [27] studied SIC behavior of the polychloroprene rubber (CR) where the polymer network is assumed to contain regular trans-CR zones surrounded by cross-linked amorphous zones. At ambient temperature, the cross-linking hinders the crystallization of CR. Large strains of the cross-link network accelerate the alignment of trans-CR segments and lead then to the SIC. In another approach, a mechanism for the SIC in a nanoclay filled rubber is proposed following the concept of the dual crystallization [28]. Accordingly, alignments of clay layers in the stretch direction are considered to decrease the chain entropy and therefore to promote the crystallization process [29].

In the present work, we propose a new micromechanical model of SIC which extends our previous network evolution concept [30–33]. Accordingly, the model describes typical inelastic effects of filled rubbers such as the Mullins effect, permanent set, and deformation-induced anisotropy. In order to exclude the TIC, lower temperatures (below the room temperature) are not considered. Coexistence of fibrillar and lamellar crystals in the shish-kebab structure is assumed [21,25,34]. Polymer chains immobilized by crystallization are subdivided into stretched and flexible chains. Thus, in addition to the classical CC and PP networks [33] two separate networks of stretched (ST) and flexed (FL) chains are introduced (Fig. 4). These networks describe the stress upturn induced by SIC.

The paper is organized as follows. In Sec. II we briefly recall the network evolution model [33] for the fully amorphous network. In Sec. III the procedure of phase transition between amorphous and crystallines is described. The constitutive formulation is further derived in Sec. IV. In Sec. V prediction capabilities of the model are evaluated in comparison with different *in situ* experimental data [34,35] for the stress-strain relation and the crystallinity evolution. In addition, restrictions on material parameters and the thermodynamic consistency of the proposed model are discussed in Appendices A and B, respectively.

II. AMORPHOUS NETWORK MODELING

A. Statistical mechanics of a single chain

We consider a polymer chain with n segments and the end-to-end distance R spanned between to aggregate surfaces. Assuming that none of the segments between number 1 and n is joined to an aggregate surface, the probability of existence

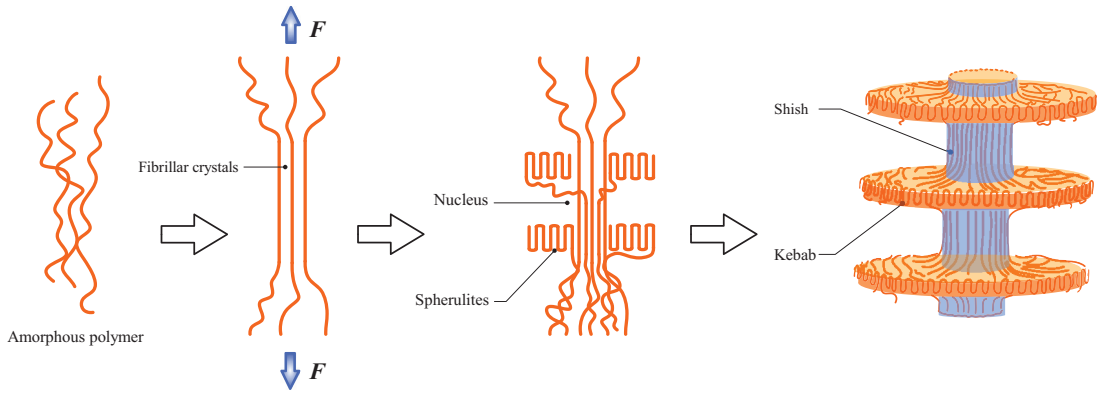

FIG. 3. (Color online) The formation of a shish-kebab crystal. The (a) amorphous polymer chains form (b) fibrillar crystals under tension, which acts as (c) a nucleus in the formation of spherulites. This procedure leads to the creation of (d) shish-kebab crystals.

of the chain is given by (see, e.g., Ref. [33])

$$P(n,\bar{R}) = \kappa\sqrt{\frac{\alpha}{\pi n}}\exp(A), \tag{1}$$

$$A = -\alpha\frac{\bar{R}^2}{n} - \kappa\sqrt{\frac{\alpha}{\pi}}\left[2\sqrt{n}\exp\left(-\alpha\frac{\bar{R}^2}{n}\right) + 2\bar{R}\sqrt{\pi\alpha}\left(\operatorname{erf}\left(\bar{R}\sqrt{\frac{\alpha}{n}}\right) - \operatorname{erf}(\bar{R}\sqrt{\alpha})\right) - 2\exp(-\alpha\ \bar{R}^2)\right], \tag{2}$$

where κ is the relative average area of active adsorption sites on the aggregate surface available for one bond and $\alpha = \frac{3}{2}$. The overbar $\bar{\bullet} = \frac{\bullet}{l}$ denotes a normalized value with respect to the segment length l.

Let us denote the position vectors of the chain ends in the reference and current configuration by $\boldsymbol{R}$ and $\boldsymbol{r}$ and their lengths by R and r, respectively. Accordingly, one has

$$\boldsymbol{r} = \mathbf{F}_m\boldsymbol{R}, \quad r = \overset{d}{\lambda}R, \tag{3}$$

where $\mathbf{F}_m$ denotes the deformation gradient in the microscale, and $\overset{d}{\lambda}$ is the microstretch in a direction specified by the unit vector $\boldsymbol{d}$. Hereafter, the following font styles are used for scalar X, vector $\boldsymbol{X}$, second-order $\mathbf{X}$, microstretch λ, and macrostretch χ.

According to the non-Gaussian statistics, the strain energy of a chain per unit referential volume of the rubber matrix is written by

$$\psi(n,\bar{r}) = nKT\left(\frac{\bar{r}}{n}\beta + \ln\frac{\beta}{\sinh\beta}\right), \tag{4}$$

where $\beta = \mathcal{L}^{-1}(\frac{\bar{r}}{n})$ and $\mathcal{L}^{-1}$ denotes the inverse Langevin function. Further, K and T denote Boltzmann's constant and absolute temperature, respectively.

A proper approximation approach for the inverse Langevin function can be chosen depending on the elongation range of polymer chains. In the case of moderate and large deformations, the Taylor expansion appears to be more favorable (see Ref. [36]). However, if chain breakage occurs in the state very close to the fully stretched state where $0.96 < \frac{\bar{r}}{n} < 13$, then rational functions, as, for example, the Padé approximant

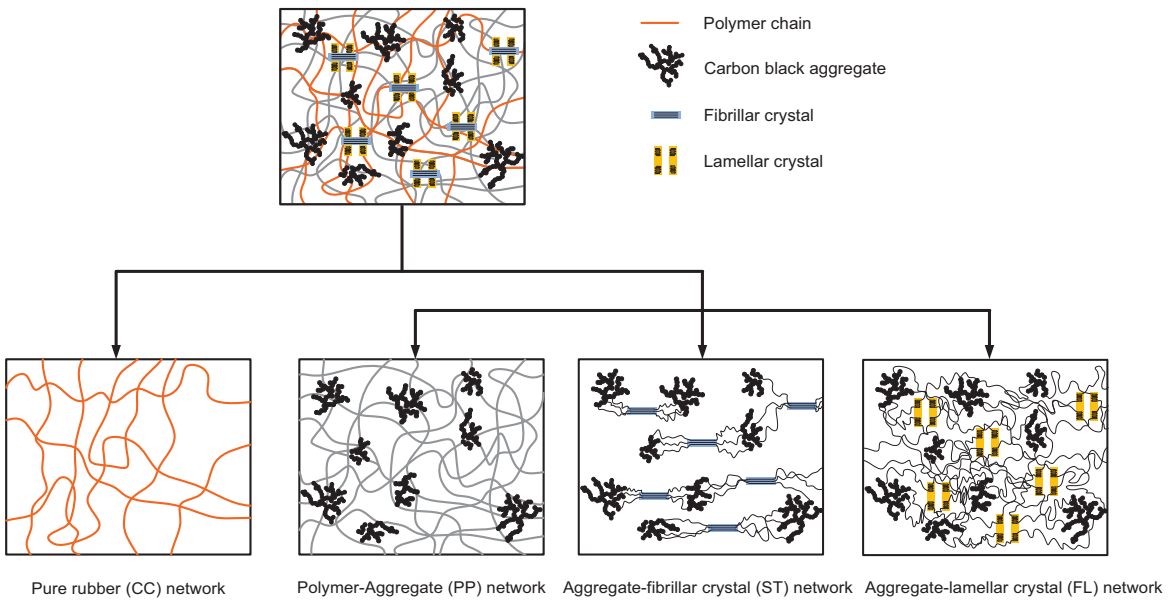

FIG. 4. (Color online) Decomposition of the rubber matrix into four networks (CC, PP, ST, and FL).

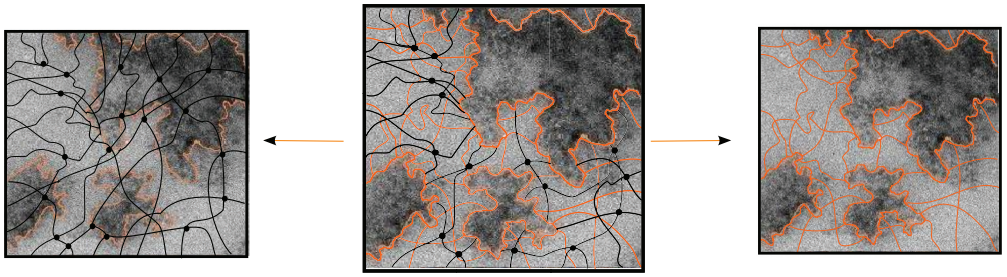

FIG. 5. (Color online) Illustration of the network decomposition concept.

$\mathcal{L}^{-1}(x) \approx \frac{3x}{1-x^3}$ [37], show better agreement with the exact values [36].

B. Strain energy of the amorphous rubber matrix

The amorphous rubber matrix is decomposed into a pure rubber network (CC) and a polymer-filler network (PP), which act parallel to each other [33,38,39]. Accordingly, the strain energy of the rubber matrix Ψ_M relative to its reference volume is represented by

$$\Psi_M = \Psi_{\rm cc} + \Psi_{\rm pp}, \tag{5}$$

where $\Psi_{\rm cc}$ and $\Psi_{\rm pp}$ denote the strain energies of the CC and PP networks, respectively (see Fig. 5).

C. Pure rubber network

The pure rubber network is considered as an ideally elastic network with affine motion of cross-links and the identical chains that are initially in the unperturbed state. Accordingly, the entropic energy of a single chain subjected to elongation is represented by (4) as $\psi(n, \overset{\boldsymbol{d}}{\chi}) = \psi(n, \overset{\boldsymbol{d}}{\chi}\bar{R}_0)$, where the microstretch $\overset{\boldsymbol{d}}{\lambda}$ is equal to the macrostretch $\overset{\boldsymbol{d}}{\chi}$. In order to obtain the strain energy of the CC network, N_c chains with n_c segments are considered in each spatial direction, so that

$$\Psi_{\rm cc} = \frac{1}{A_s}\int_S N_c \psi\left(n_c, \overset{\boldsymbol{d}}{\chi}\right) d\overset{\boldsymbol{d}}{s}, \tag{6}$$

where A_s represents the surface area of the microsphere and $d\overset{\boldsymbol{d}}{s}$ is an infinitesimal area of a surface with the normal direction $\boldsymbol{d}$.

D. Polymer-filler network

The evolution of the polymer-filler network is assumed to be responsible for damage in rubber. Let $\tilde{N}(n,\bar{r})$ be the number of chains with the number of segments (relative length) n and the relative end-to-end distance $\bar{r}$. The integration over the whole set D_A of chains available in the direction specified by the unit vector $\boldsymbol{d}$ yields the free energy of chains in this direction as

$$\overset{\boldsymbol{d}}{\Psi} = \int_{D_A} \tilde{N}(n,\bar{r})\psi(n,\bar{r})dn. \tag{7}$$

The network evolution concept considers aggregate-polymer debonding and network rearrangement as two simultaneous interacting processes. In the course of deformation, polymer chains begin to slide on or debond from aggregates. This debonding starts with the shortest chain and gradually involves longer and longer chains. Under unloading, the debonded chains do not reattach back to the aggregates and, thus, the maximal microstretch previously reached in the loading history

$$\overset{\boldsymbol{d}}{\lambda}_{\max} = \max_{\tau\in(-\infty,t]} \overset{\boldsymbol{d}}{\lambda}(\tau) \tag{8}$$

is crucial for the description of the polymer-filler debonding [40, cf. 41]. Accordingly, the length of the shortest available chain in the deformed subnetwork is then obtained by

$$n_{\min}\left(\overset{\boldsymbol{d}}{\lambda}_{\max}\right) = \nu \overset{\boldsymbol{d}}{\lambda}_{\max}\bar{R}, \tag{9}$$

where $\nu > 1$ denotes a sliding ratio treated as a material parameter.

Furthermore, we assume an upper limit for the length of a chain between two aggregates, denoted in the following by $n_{\max}$ (for details see Ref. [33]). Accordingly, the set of available relative lengths of chains bounded to aggregates in the direction $\boldsymbol{d}$ can be expressed by

$$D_A\left(\overset{\boldsymbol{d}}{\lambda}_{\max}\right) = \{n | n_{\min} \leqslant n \leqslant n_{\max}\}. \tag{10}$$

The concept of chain rearrangement in rubber network suggests that the total number of active segments remains constant [33]. This assumption yields

$$\tilde{N}(n,\bar{r}) = N_0\Phi\left(\overset{\boldsymbol{d}}{\lambda}_{\max}\right)P(n,\bar{R}) = N_0\Phi\left(\overset{\boldsymbol{d}}{\lambda}_{\max}\right)\hat{P}(n), \tag{11}$$

where

$$\Phi(x) = \left(\int_{D_A(x)} \hat{P}(n)ndn\right)^{-1}. \tag{12}$$

We consider $\bar{R}$ as a material constant and denote $\hat{P}(n) = P(n,\bar{R})$. N_0 represents the number of active chains per unit undeformed volume and will also be considered as a material parameter. Finally, considering (11) and (10) in (7), the energy of a subnetwork in direction $\boldsymbol{d}$ is expressed by

$$\overset{\boldsymbol{d}}{\Psi} = N_0\Phi\left(\overset{\boldsymbol{d}}{\lambda}_{\max}\right)\int_{D_A\left(\overset{\boldsymbol{d}}{\lambda}_{\max}\right)} \hat{P}(n)\psi\left(n, \overset{\boldsymbol{d}}{\lambda}\bar{R}\right)dn. \tag{13}$$

E. Strain amplification

In filled rubbers, the stretch applied to the polymer chains is referred to as microstretch. It is usually larger than the stretch applied to the rubber matrix referred to as macro-stretch. Thus, the inhomogeneity of the material leads to the inhomogeneity in the micro-stretch distribution [20]. Accordingly, an amplification function X establishing a relationship between the microstretch $\overset{\boldsymbol{d}}{\lambda}$ and the macrostretch $\overset{\boldsymbol{d}}{\chi}$ is defined by

$$\overset{\boldsymbol{d}}{\lambda} = X\left(\overset{\boldsymbol{d}}{\chi}\right) = \frac{\overset{\boldsymbol{d}}{\chi} - C^{\rm p}}{1 - C^{\rm p}}, \tag{14}$$

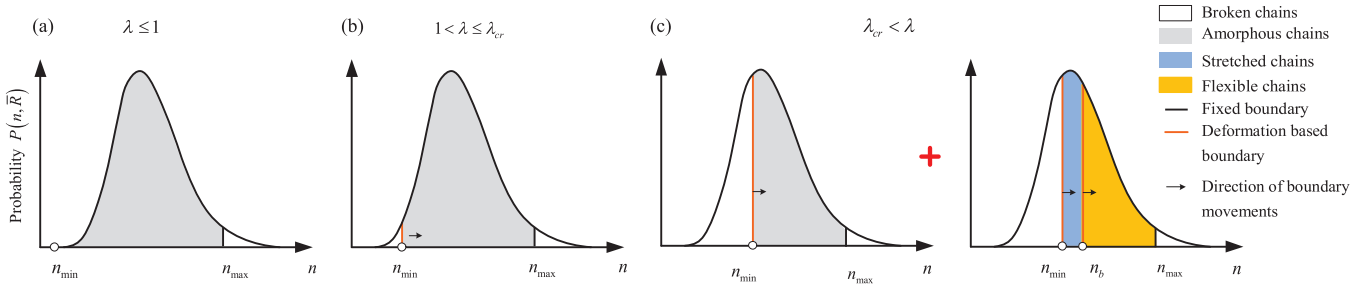

FIG. 6. (Color online) Evolution of different chain types under deformation: (a) amorphous phase in the virgin state, (b) debonding of shorter chains before crystallization, and (c) formation of the semicrystallized phase besides the amorphous phase.

where $C \in (0,1)$ represents the volume fraction of filler per unit volume of rubber matrix ($C < 0.3$ in most studies), while $\mathfrak{p}$ depends on the structure of the filler network. Bueche [42] showed that the constant $\mathfrak{p} = \frac{1}{3}$ in the case of a statistically homogeneous distribution of spherical particles (see, for example, Refs. [43,44]). The influence of $\mathfrak{p}$ and C on the material parameters $\{\kappa, R, n_{\max}\}$ has been discussed in Ref. [31]. Let us represent parameters related to fillers, polymers, crystals, additives, and the rubber matrix by the subscripts f, p, c, a, and r, respectively. Then

$$C = \frac{V_f}{V_r}, \quad V_r = V_f + V_p + V_a, \tag{15}$$

where V denotes the volume.

III. STRAIN-INDUCED CRYSTALLIZATION

A. Crystallization

We denote a stretch at which the formation of the crystals begins under loading by $\chi_{\rm cr}$ and a stretch at which the last crystal melts under unloading by $\chi_{\rm ml}$. These values depend on the temperature and the compound.

Before crystallization, all polymer chains in the rubber matrix are in the amorphous phase. With the onset of crystallization, some parts of amorphous polymer chains crystallize [24,46]. These polymer chains are referred in the following to as semicrystallized chains.

In order to model the nucleation of crystals during SIC, the semicrystallized polymer chains are further categorized into stretched and flexible chains according to their flexibility ratio ($\frac{n}{\bar{r}}$). The stretched chains are highly elongated chains forming fibrous crystals that act as a nucleus for the creation of spherulites. The flexible chains, on the other hand, participate in the formation of the spherulites by folding back and forth into the spherulites lamellae (kebab structures). The flexible and stretched chains can frequently transform into each other, as observed by the back-and-forth conversion of the spherulites to and back from the fibrillar crystals under loading and unloading [47].

Let us further denote the critical flexibility ratio that specifies the boundary between stretched and flexible chains by a_b. Accordingly, the following chain decomposition holds under loading:

Loading condition	$\lambda \leqslant 1$	$1 < \lambda \leqslant \lambda_{\rm cr}$	$\lambda_{\rm cr} < \lambda$
State of chain	$n_{\min} < n$ amorphous	$n_{\min} \geqslant n$ broken $n_{\min} < n$ amorphous	$n_{\min} \geqslant n$ broken $n_{\min} < n \leqslant n_b$ stretched $n_b < n$ flexible

(16)

where $n_b = a_b \lambda_{\max} \bar{R}$ and $\lambda_{\rm cr}$ is the microstretch (corresponding to the macrostretch $\chi_{\rm cr}$) at the onset of crystallization.

Thus, the set of active stretched $D_{\rm st}$ and flexible $D_{\rm fl}$ chains can be represented by

$$D_{\rm st} = \{n | n_{\min} \leqslant n \leqslant n_b\},$$
$$D_{\rm fl} = \{n | n_b < n \leqslant n_{\max}\}. \tag{17}$$

In the course of deformation, shorter chains begin to debond from aggregates and the number of active chains decreases (see Fig. 6), which leads to the stress softening. When the micro-stretch ratio reaches $\lambda_{\rm cr}$, SIC takes place almost instantaneously [45] and some amorphous chains convert into semicrystallized chains [24,46]. The volume ratio of the crystals to the whole matrix

$$\zeta = \frac{\text{number of crystallized segments}}{\text{total number of segments}} \tag{18}$$

is referred to as the degree of crystallization.

Experimental results show that only a small number of polymer chains are crystallized under extension [22,24,46]. By denoting the fraction of the crystal phase as η, the strain energy of the rubber matrix ψ_M can be expressed by [48,49]

$$\Psi_M = \Psi_{\rm cc} + (1-\eta)\Psi_{\rm pp} + \eta(\Psi_{\rm st} + \Psi_{\rm fl}), \tag{19}$$

where $\Psi_{\rm st}$ and $\Psi_{\rm fl}$ denote the strain energy of semicrystallized stretched and flexible chains, respectively. It is seen that (19) is a generalization of (5) for $\eta > 0$.

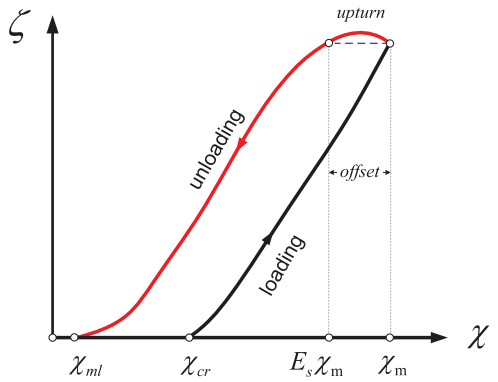

FIG. 7. (Color online) A schematical diagram of the crystallization degree in the first loading cycle versus macrostretch. Last crystal melts at $\chi_{\rm ml}$, the residual crystals at the stress-free state are referred to as elastic set.

B. Decrystallization

The fibrillar crystals melt first; the melting process starts with the longest crystal and continues with shorter ones. The last crystal melts at $\chi_{\rm ml}$ (Fig. 7). Disappearance of the nucleus in the shish-kebab is then followed by melting of the spherulites and partial release of the semicrystallized flexible chains [47].

Slight disorientation of crystallites during unloading [25,50] suggests that the melting process has no directional preferences. Similarly to the crystallization, the melting process is also assumed to be governed by chain length distribution (see Fig. 8). The crystallization degree at the beginning of the unloading is influenced by both melting of the lamellar crystals and transformation of the fibrillar crystals into the lamellar ones [46]. Thus, due to the fact that the melting rate of lamellar crystals is higher than their formation rate, the degree of crystallization is expected to decrease during unloading [51]. However, some polymers demonstrate higher formation rate at the beginning of the unloading [35], which leads to a bump in the crystallization degree graph (see Fig. 7). In this case, the dominant melting procedure might not start immediately with the unloading where $\lambda = \lambda_m$ but after an offset E_S, such that the melting starts at $\lambda = E_s\lambda_{\max}$ (see Fig. 7).

Thus, under unloading, polymer chains can be categorized as follows:

Loading condition	$\lambda_{\rm ml} < \lambda$		$\lambda \leqslant \lambda_{\rm ml}$	
State of chain	$n_{\min} \geqslant n$	broken	$n_{\min} \geqslant n$	broken
	$n_{\min} < n \leqslant n_m$	stretched	$n_{\min} < n$	amorphous
	$n_m < n \leqslant n_b$	amorphous (melted)		
	$n_b < n$	flexible + amorphous		

(20)

where $\lambda_{\rm ml}$ is the microstretch corresponding to the macrostretch $\chi_{\rm ml}$ and n_m represents the relative length of the shortest melted chain. The flexibility ratio $a_m = \hat{a}_m(\lambda)$ can be expressed from the condition $n_m = \hat{a}_m(\lambda)\bar{R}$.

Thus, the sets of active stretched $D_{\rm st}$ and flexible $D_{\rm fl}$ chains are given under unloading by

$$D_{\rm st} = \{n|n_{\min} \leqslant n \leqslant n_m\}, \quad D_{\rm fl} = \{n|n_b < n \leqslant n_{\max}\}. \quad (21)$$

C. Strain energy of stretched chains

At the onset of the melting procedure $n_m = n_b$ at $\lambda = E_s\lambda_{\max}$(see Fig. 8). Thus,

$$a_m\bar{R}|_{\lambda=E_s\lambda_{\max}} = a_b\lambda_{\max}\bar{R} \quad \Rightarrow \quad a_m|_{E_s\lambda_{\max}} = a_b\lambda_{\max}. \quad (22)$$

Taking into account that the last crystal melts at $\lambda_{\rm ml}$, one obtains

$$a_m|_{\lambda_{\rm ml}} = \nu\lambda_{\max}. \quad (23)$$

For the sake of simplification, a_m can be represented by a linear function which can be expressed in view of (22) and (23) as

$$a_m = \hat{a}_m(\lambda) = a_b\lambda_{\max} - (E_s\lambda_{\max} - \lambda)\frac{a_b\lambda_{\max} - \nu\lambda_{\max}}{E_s\lambda_{\max} - \lambda_{\rm ml}}. \quad (24)$$

Since the crystallization degree under unloading is higher than under loading (see Fig. 7), one has $n_m|_{\lambda_{\max}} > n_b$, which can be satisfied by setting $a_b > \nu$ (see Appendix A for further details). Accordingly, in view of (17) and (21), $D_{\rm st}$ in each direction can be given as

$$D_{st} = \{n|n_{\min} < n < \max[\min\{n_m,n_b\},n_{\min}]\}, \quad (25)$$

where $\min\{n_m,n_b\}$ represents the length of the longest crystallized stretched chain, and $\max[\min\{n_m,n_b\},n_{\min}]$ is to guarantee that this length cannot become smaller than the length of the shortest amorphous chain.

Experimental observations show that the crystallite sizes remain almost constant during deformation [24,25,46]. Thus, SIC mainly develops through the nucleation of new crystals rather than through the growth of the existing crystallites [51]. The constant crystallite size can be taken into account by considering the ratio

$$I_c = \frac{\text{crystallized segments of a chain}}{\text{total segments of a chain}} \quad (26)$$

as a material constant.

In the following we assume that the fibrillar crystal forms in the middle of the stretched chain in its end-to-end direction [Fig. 9(c)]. Since the crystallite sizes are constant, the energy contribution of the crystallized part of the chain were neglected. However, crystallites are considered as conceptual cross-links [12,13] and thus influence the entropic contribution of semicrystallized chains. Accordingly, the entropic energy

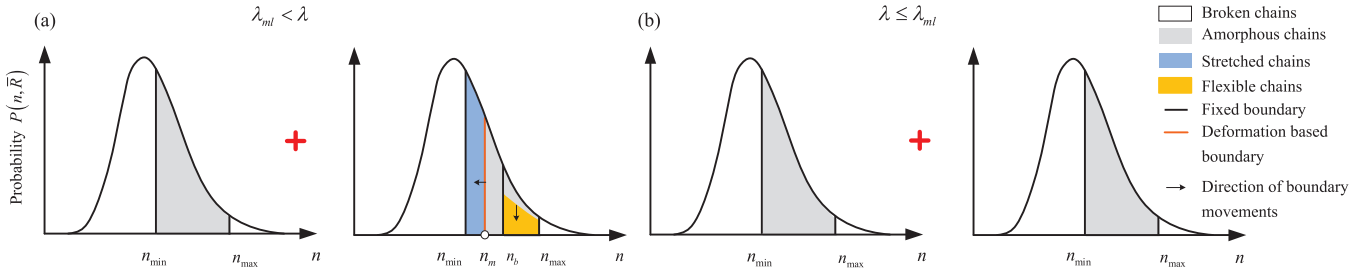

FIG. 8. (Color online) Evolution of the polymer chain types during unloading: (a) amorphous and semicrystallized phases and (b) melting completed, no crystals.

of the amorphous part can be given by [52, cf. (4)]

$$\psi^{\mathrm{st}}(n,\bar{r}) = \psi^{c}\left(n^{\mathrm{st}}, \frac{(\lambda\bar{R} - nI_c)}{2}\right), \tag{27}$$

where $n^{\mathrm{st}} = \frac{n(1-I_c)}{2}$. Thus, in view of (13), the total strain energy of stretched chains in a direction $\boldsymbol{d}$ is given by $N_0\Phi(\lambda_{\max})\int_{D_{\mathrm{st}}} 2\hat{P}(n)\psi^{\mathrm{st}}(n,\lambda\bar{R})dn$. During unloading, some of those stretched chains melt and become amorphous again [see Fig. 8(a)]. The domain of these amorphous chains is given by

$$D_{\mathrm{am}} = \{n|\,\max[\min\{n_m,n_b\},n_{\min}] < n < \max[n_b,n_{\min}]\}. \tag{28}$$

The fraction of fibrillar crystals in the direction $\boldsymbol{d}$ can further be expressed by

$$g^{\mathrm{st}}(\boldsymbol{d}) = \begin{bmatrix} 0 & \text{if } \lambda \leqslant \lambda_{\mathrm{cr}} \wedge \dot{\lambda} > 0 \\ \frac{N^{\mathrm{st}}(\boldsymbol{d})}{N^{\mathrm{st}}_{\max}(\boldsymbol{d})} & \text{otherwise} \end{bmatrix}, \tag{29}$$

where

$$N^{\mathrm{st}}(\boldsymbol{d}) = N_0\int_{D_{st}} \phi(\lambda_m)\hat{P}(n)dn,$$
$$N^{\mathrm{st}}_{\max}(\boldsymbol{d}) = \max_{\tau\in(-\infty,t]} N^{\mathrm{st}}(\boldsymbol{d}) \tag{30}$$

denote the number of fibrillar crystals in the direction $\boldsymbol{d}$ and the maximum number of previously formed fibrillar crystals, respectively. Thus, the entropic energy of a semicrystallized subnetwork of stretched chains in a direction $\boldsymbol{d}$ can be expressed for the complete loading cycle by

$$\overset{\boldsymbol{d}}{\Psi}_{\mathrm{st}} = N_0\Phi(\lambda_{\max})\Big[g^{\mathrm{st}}\int_{D_{\mathrm{st}}} 2\hat{P}(n)\psi^{\mathrm{st}}(n,\bar{r})dn + [1-g^{\mathrm{st}}]\int_{D_{\mathrm{am}}} \hat{P}(n)\psi(n,\bar{r})dn\Big], \tag{31}$$

where the second term represents the entropic energy of melted chains. This term is zero during loading, since $n_b = \min\{n_{\mathrm{m}},n_b\}$.

D. Strain energy of flexible chains

At the onset of crystallization, a flexible chain is converted into two smaller chains and a lamellar crystal in the plane normal to the fibrillar crystal [Fig. 9(b)]. Experimental results show that most of crystallites are oriented in the extension direction [24,46,51,53,54]. We also assume that the lamellar crystals form at the middle of the interaggregates distance [Fig. 9(d)]. By neglecting the thickness of the lamellar crystal, one can thus express the end-to-end vectors of the two

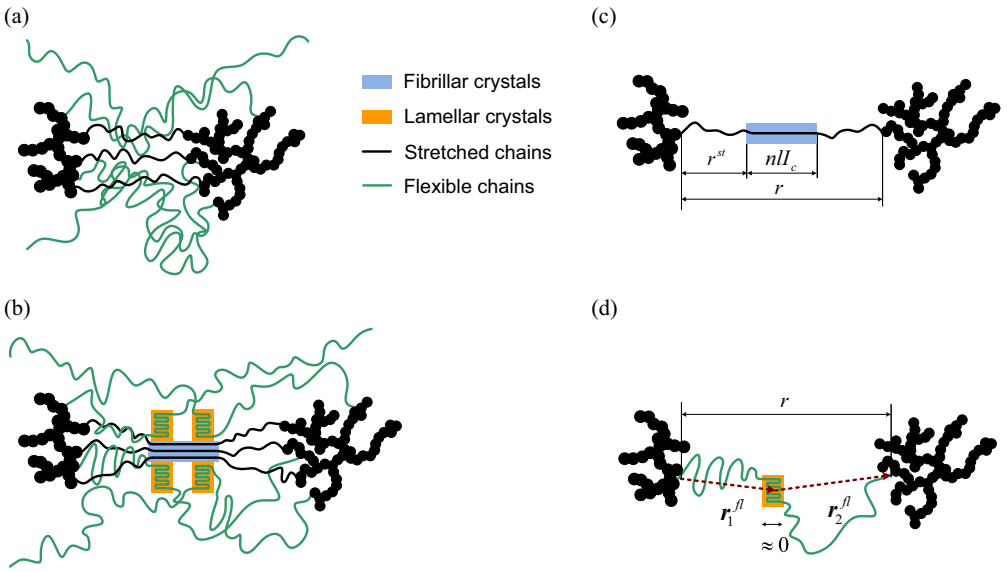

FIG. 9. (Color online) Semicrystallized ST and FL chains: (a) the virgin rubber matrix, (b) onset of crystallization, (c) formation of ST chains from stretched chains, and (d) formation of FL chains from flexible chains.

newly created flexible chains as $\bar{r}_1^{\mathrm{fl}} = \bar{r}_2^{\mathrm{fl}} = \frac{\bar{r}}{2} = \frac{\overset{d}{\lambda}\bar{R}}{2}$, where $\bar{r}_i^{\mathrm{fl}} = \|\bar{\boldsymbol{r}}_i^{\mathrm{fl}}\|$.

The energy of an FL chain in a direction $\boldsymbol{d}$ can be given by

$$\psi^{\mathrm{fl}}(n,\bar{r}) = \psi\left(n^{\mathrm{fl}}, \overset{d}{\lambda}\frac{\bar{R}}{2}\right), \tag{32}$$

where $n^{\mathrm{fl}} = \frac{n(1-I_C)}{2}$ denotes the number of segments.

Under simultaneous melting of fibrillar and lamellar crystals, their fractions in a direction $\boldsymbol{d}$ are equal so that

$$g^{\mathrm{fl}}(\boldsymbol{d}) = g^{\mathrm{st}}(\boldsymbol{d}),$$

where $g^{\mathrm{st}}(\boldsymbol{d})$ is defined by (29). Thus, in view of (31), the energy of a semicrystallized subnetwork of flexible chains in the direction $\boldsymbol{d}$ can be represented by

$$\overset{d}{\Psi}_{fl} = N_0\Phi(\lambda_{\max})\left[g^{\mathrm{st}}\int_{D_{\mathrm{fl}}} 2\hat{P}(n)\psi^{\mathrm{fl}}(n,\bar{r})dn + [1-g^{\mathrm{st}}]\int_{D_{\mathrm{fl}}}\hat{P}(n)\psi(n,\bar{r})dn\right], \tag{33}$$

where the last term describes the entropic energy of melted chains.

IV. CONSTITUTIVE MODELING

A. 3D generalization

Assuming an initially isotropic spatial distribution of polymer chains in the rubber matrix, the macroscopic energy of a three-dimensional network can be obtained similarly to (6) by the integration over the unit sphere as

$$\Psi_{\mathrm{pp}} = \frac{1}{A_s}\int_S \overset{d}{\Psi}\, d\overset{d}{s}, \quad \Psi_{\mathrm{st}} = \frac{1}{A_s}\int_S \overset{d}{\Psi}_{\mathrm{st}} d\overset{d}{s}, \quad \Psi_{\mathrm{fl}} = \frac{1}{A_s}\int_S \overset{d}{\Psi}_{\mathrm{fl}} d\overset{d}{s}. \tag{34}$$

The integration is carried out numerically by

$$\Psi_{\mathrm{cc}} \approx N_c\sum_{i=1}^{k}\psi\left(n_c, \overset{d_i}{\chi}\right)w_i, \quad \Psi_{\mathrm{pp}} \approx \sum_{i=1}^{k}\overset{d_i}{\Psi}\, w_i, \quad \Psi_{\mathrm{st}} \approx \sum_{i=1}^{k}\overset{d_i}{\Psi}_{\mathrm{st}}\, w_i, \quad \Psi_{\mathrm{fl}} \approx \sum_{i=1}^{k}\overset{d_i}{\Psi}_{\mathrm{fl}}\, w_i, \tag{35}$$

where w_i are weight factors corresponding to the collocation directions $\boldsymbol{d}_i\,(i = 1,2,\ldots,k)$. In this study, we utilize the numerical scheme by Heo and Xu [55] which was shown by Ehret *et al.* [56] to provide the best trade-off between the least error with respect to the induced anisotropy and the computational costs. Accordingly, a set of $k = 45$ integration points on the half sphere is chosen, and the coordinate of an arbitrary point i in the orthogonal basis is represented by the unit vector $\boldsymbol{d}_i$. Substitution of (13) and (31) into (35) yields the energy of the rubber matrix as

$$\begin{aligned}\Psi_M = \Psi_{\mathrm{cc}} + (1-\eta)\Psi_{\mathrm{pp}} + \eta(\Psi_{\mathrm{st}} + \Psi_{\mathrm{fl}}) &= N_c\sum_{i=1}^{k} w_i\psi\left(n_c, \overset{d_i}{\chi}\right) + (1-\eta)N_0\sum_{i=1}^{k} w_i\int_{D_A}\Phi\left(\overset{d_i}{\lambda}_{\max}\right)\hat{P}(n)\psi\left(n, \overset{d_i}{\lambda}\bar{R}\right)dn \\ &+ \eta N_0\sum_{i=1}^{k} w_i\Phi\left(\overset{d_i}{\lambda}_{\max}\right)\left[g^{st}\int_{D_{\mathrm{st}}} 2\hat{P}(n)\psi^{\mathrm{st}}(n,\bar{r})dn + [1-g^{\mathrm{st}}]\int_{D_{\mathrm{am}}}\hat{P}(n)\psi(n,\bar{r})dn\right] \\ &+ \eta N_0\sum_{i=1}^{k} w_i\Phi\left(\overset{d_i}{\lambda}_{\max}\right)\left[g^{\mathrm{st}}\int_{D_{\mathrm{fl}}} 2\hat{P}(n)\psi^{\mathrm{fl}}(n,\bar{r})dn + [1-g^{\mathrm{st}}]\int_{D_{\mathrm{fl}}}\hat{P}(n)\psi(n,\bar{r})dn\right].\end{aligned} \tag{36}$$

Before the onset of crystallization, the total network energy (36) reduces to the simple form according to the network evolution model [33] for purely amorphous systems.

B. Evolution of the crystallization degree

In view of the constant length of crystals during deformation, ζ can be considered to be proportional to the crystal fraction of each chain I_c, to the number of fibrillar crystals N^{ST} in the matrix, and to $\frac{\langle n\rangle}{n_{\mathrm{all}}}$, where $\langle n\rangle$ denotes the average number of chain segments in one chain while n_{all} is the total number of segments. The latter two values do not change under deformation. Accordingly, one can write

$$\zeta \propto I_c N^{\mathrm{ST}}\frac{\langle n\rangle}{n_{\mathrm{all}}} \quad \Rightarrow \quad \zeta = \zeta_0 N^{\mathrm{ST}}, \tag{37}$$

where ζ_0 denotes a material constant, and the total number of fibrillar crystals in the network N^{ST} is calculated as

$$N^{\mathrm{ST}} = \frac{\eta}{A_s}\int_S N^{\mathrm{st}}(\boldsymbol{d})d\overset{d}{s}. \tag{38}$$

C. Macroscale behavior

While filled rubber is normally treated as an incompressible material, strain-induced crystallite may change its macroscopic volume. However, there has been very less experimental evidence confirming the compressibility of filled rubber undergoing SIC (see, e.g., Ref. [57]). In the current model we assume that the amorphous matter and the crystallite part in the rubber matrix keep the same density under deformation [58–60]. Taking into account the incompressibility condition $\det\mathbf{F} = 1$, we can now obtain the constitutive equation for the first Piola-Kirchhoff stress tensor by

$$\mathbf{P} = \frac{\partial\Psi}{\partial\mathbf{F}} - p\mathbf{F}^{-T}, \tag{39}$$

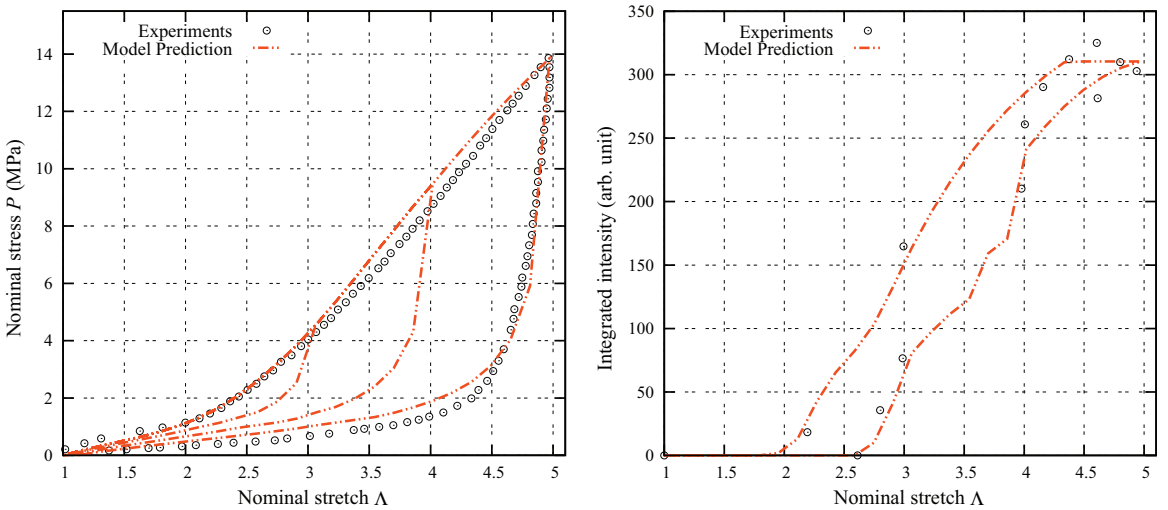

FIG. 10. (Color online) Comparison of the model prediction with the experimental data on uniaxial tension of 40phr NR: (a) stress-stretch relation and (b) integrated intensity (proportional to the crystallization degree ζ) versus stretch ratio.

where p denotes an unknown parameter related to the hydrostatic pressure and Ψ is given by (36). The derivative of this expression is obtained by means of the chain rule of differentiation and by using the following identities:

$$\frac{\partial \overset{d_i}{\lambda}}{\partial \overset{d_i}{\chi}} = \frac{1}{1-C^{\mathfrak{p}}}, \quad \frac{\partial \overset{d_i}{\chi}}{\partial \mathbf{F}} = \frac{\partial \boldsymbol{d}_i \mathbf{C} \boldsymbol{d}_i}{\partial \mathbf{F}} = 2\mathbf{F}\mathbf{D}_i,$$

where $\mathbf{D}_i = \boldsymbol{d}_i \otimes \boldsymbol{d}_i,$ (40)

$$\frac{\partial \psi(n,x)}{\partial x} = \sqrt{n} K T \mathcal{L}^{-1}\left(\frac{x}{\sqrt{n}}\right). \quad (41)$$

V. EXPERIMENTAL EVALUATION

In this section, the model predictions are compared with the results of *in situ* experiments on samples with two different filler concentrations, N339 40phr [35] and N234 45phr [34]. In these experiments unaxial tension cycles with increasing stretch amplitudes of 3.0, 4.0, 5.0 and 2.75, 3.3, 3.75 were performed for both filler concentrations. The experimental data are presented in Figs. 10 and 11, respectively. There, the nominal stress P and the so-called integrated intensity of the crystallization halo which is proportional to the crystallization degree ζ are plotted versus stretch Λ.

The model was fitted to these experimental data by means of 10 material parameters listed in Table I. To this end, the least-squares error criterion both with respect to the stress-stretch and crystallization-stretch results was utilized. The least-squares residual was minimized with the aid of the Levenberg-Marquardt algorithm. First, the values of a_b, I_c, and ζ_0 are approximated using the crystallization-stretch graph. Then the parameters of the network evolution model

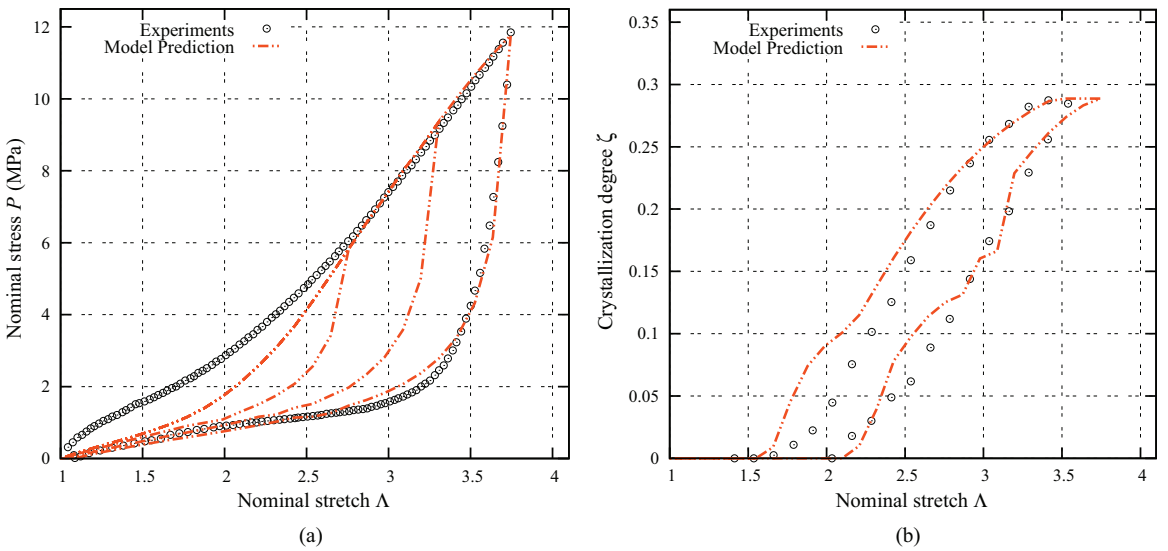

FIG. 11. (Color online) Comparison of the model prediction with the experimental data on uniaxial tension of 45phr NR: (a) stress-stretch relation and (b) crystallization degree versus stretch ratio.

TABLE I. Material parameters found in the fitting procedure.

	Network evolution model							SIC model		
Material	κ	ν	$\bar{R}$	$n_{\max}$	n_c	$\tilde{N}_0 KT$	$\tilde{N}_c KT$	a_c	I_c	ζ_0
NR-40H	55.18	1.0088	17.52	250	80	8.522[MPa]	0.01[MPa]	1.15	0.2	660e3
NR-45	450	1.0208	19.52	200	80	6.622[MPa]	0.01[MPa]	1.18	0.2	431

are approximated by fitting to the stress-stretch relation. The obtained values were then further improved by recursive application of the aforementioned fitting procedure.

The so-obtained material parameters are given in Table I. The other physical values were directly taken from experimental measurements (see Table II). The resulting stress-stretch and crystallization-stretch curves predicted by the model are plotted in Figs. 10 and 11 against the experimental data. For both filled rubbers one can observe good agreement with respect to the stress-stretch relation as well as evolution of crystallinity.

The parameters $\{\kappa, R, n_{\max}\}$ are directly influenced by the filler concentration and $\{\nu, a_c\}$ by the type of filler. The parameters $\{n_c, \tilde{N}_0, \tilde{N}_c\}$ depend on the cross-linking and monomer properties. The value of the crystallized segment fraction in a polymer chain I_c belongs to the range 20–25% known from the literature [21].

VI. CONCLUSIONS

A micromechanical model for the strain-induced crystallization of filled rubbers has been presented in this paper. The model extends the previously proposed network evolution model and takes thus other inelastic effects of filled rubbers into account such as permanent set, stress softening, and induced anisotropy. The model subdivides semicrystallized polymer chains into stretched chains that form fibrillar crystals and into flexible chains that form lamellar crystals. Accordingly, two networks of stretched and flexible chains are introduced in addition to the classical CC and PP networks. The stress upturn resulting from the crystalline nucleation is well predicted by the model. The model is described by a relative few number of additional material constants and demonstrates good agreement with experimental data both with respect to the stress-stretch and crystalization-stretch behavior.

ACKNOWLEDGMENT

The financial support of German Research Foundation (DFG) is gratefully acknowledged.

TABLE II. Experimentally measured physical model parameters for rubbers with different filler contents.

Material	χ_{cr}	χ_{ml}	E_s	C	η
NR-40H	2.6	1.9	0.85	0.20	0.28
NR-45	2.1	1.5	0.9	0.22	0.28

APPENDIX A: CRYSTALLIZATION AND MELTING CONDITIONS

According to the experimental observations the crystallization degree in unloading ($\dot{\lambda} < 0$) is higher than in loading ($\dot{\lambda} > 0$) (see Fig. 7). In this section we prove that our model satisfies this condition if we set $a_b \geqslant \nu$ (see Sec. III C). This ensures also the conditions crystallization and melting (see Figs. 6 and 8).

In an unloading direction ($\dot{\lambda} < 0$) the function a_m is linearly increasing with λ, so below the stretch value $E_s\lambda_{\max}$ (Fig. 12) we have

$$a_b\lambda_{\max} = a_m(E_s\lambda_{\max}) \geqslant a_m(\lambda), \tag{A1}$$

which leads to $n_b \geqslant n_m$ after the onset of melting. Substitution into (25) gives $D_{\text{st}} = \{n | n_{\min} < n < n_m\}$ (in accord with Fig. 8). Above $E_s\lambda_{\max}$ the formation rate is larger than the melting rate, so that $n_m \geqslant n_b$ (Fig. 12).

Next, we show that the condition $a_b \geqslant \nu$ also ensures that $n_m \geqslant n_b$ and, consequently, $D_{\text{st}} = \{n | n_{\min} < n < n_b\}$ in a loading direction ($\dot{\lambda} > 0$) (in accord with Fig. 6). Indeed, before the onset of crystallization $a_b = \nu$ and $\lambda_m = \lambda_{\max}$. Inserting these conditions into (24) yields

$$\hat{a}_m(\lambda) = a_b\lambda_{\max}. \tag{A2}$$

After the the onset of crystallization in a loading direction $a_b > \nu$, $\lambda = \lambda_{\max}$, and $E_s \leqslant 1$. Thus,

$$a_m(\lambda) = a_b\lambda_{\max} - (E_s\lambda_{\max} - \lambda)\frac{a_b\lambda_{\max} - \nu\lambda_{\max}}{E_s\lambda_{\max} - \lambda_{\text{ml}}} \geqslant a_b\lambda_{\max}. \tag{A3}$$

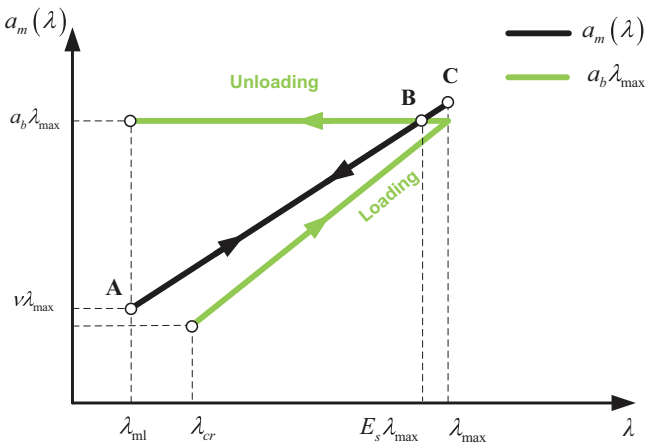

FIG. 12. (Color online) Flexibility ratio a_m and a_b versus stretch.

Combination of (A2), (A3), and (A1) gives

$$\begin{aligned} n_m &\geqslant n_b \forall \lambda | \dot{\lambda} > 0 \\ n_m &< n_b \forall \lambda | \dot{\lambda} < 0 \wedge \lambda < E_s \lambda_{\max}, \end{aligned} \tag{A4}$$

where

$$a_b = \begin{bmatrix} \nu & \text{if } \lambda \leqslant \lambda_{\rm cr} \wedge \dot{\lambda} > 0 \\ a_b > \nu & \text{otherwise} \end{bmatrix}. \tag{A5}$$

APPENDIX B: THERMODYNAMICAL CONSISTENCY

The strain energy of the rubber matrix depends on $\overset{\boldsymbol{d}_i}{\lambda}{}_{\max}$, which represent internal variables. Thus, one can write

$$\Psi_M = \Psi_M(\mathbf{C}, \Omega), \tag{B1}$$

where

$$\Omega = \left\{ \overset{\boldsymbol{d}_i}{\lambda}{}_{\max} : \boldsymbol{d}_i \in \mathcal{E}^3 \wedge \|\boldsymbol{d}_i\| = 1 \right\} \tag{B2}$$

and $\mathcal{E}^3$ denotes the three-dimensional Euclidean space (see, e.g., Ref. [61]). Accordingly, the Clausius-Duhem inequality resulting from the second law of thermodynamics reduces to $-\frac{\partial \Psi_M}{\partial \lambda_{\max}} \dot{\lambda}_{\max} \leqslant 0$. Under unloading $\dot{\lambda}_{\max} = 0$, while $\dot{\lambda}_{\max} > 0$ in the primary loading. Thus the above condition is satisfied if in the primary loading

$$-\frac{\partial \Psi_M}{\partial \lambda_{\max}} \leqslant 0 \tag{B3}$$

in all directions. In view of (36),

$$\frac{\partial \psi_{\rm pp}}{\partial \lambda_{\max}} \leqslant 0, \quad \frac{\partial \psi_{\rm st}}{\partial \lambda_{\max}} + \frac{\partial \psi_{\rm fl}}{\partial \lambda_{\max}} \leqslant 0 \tag{B4}$$

are sufficient conditions for (B3). We will prove (B4) for an arbitrary direction $\boldsymbol{d}_i$.

For the sake of brevity we write in the following x instead of $\overset{\boldsymbol{d}_i}{\lambda}{}_{\max}$. The first condition in (B4)

$$\frac{\partial}{\partial x} \int_{n_{\min}(x)}^{n_{\max}} \Phi(x) \hat{P}(n) \psi(n, \lambda \bar{R}) dn \leqslant 0 \tag{B5}$$

has been proved in Ref. [31]. Here, we focus on the second condition in (B4).

Taking into account that under the primary loading

$$\max[\min\{n_m, n_b\}, n_{\min}] = \max[n_b, n_{\min}], \quad g_{\rm st} = 1, \tag{B6}$$

the inequality $(\text{B4})_2$ can further be expressed by

$$\begin{aligned} &\frac{\partial}{\partial x} \int_{n_{\min}(x)}^{n_b(x)} \Phi(x) 2 \hat{P}(n) \psi^{\rm st}(n, \lambda \bar{R}) dn \\ &+ \frac{\partial}{\partial x} \int_{n_b(x)}^{n_{\max}} \Phi(x) 2 \hat{P}(n) \psi^{fl}(n, \lambda \bar{R}) dn \leqslant 0, \end{aligned} \tag{B7}$$

In view of (B5), $\frac{\partial}{\partial x} \int_{n_b(x)}^{n_{\max}} \Phi(x) 2 \hat{P}(n) [\psi^{\rm fl}(n, \lambda \bar{R}) - \psi^{\rm st}(n, \lambda \bar{R})] dn \leqslant 0$ holds since $n_b(x) = \frac{a_b}{\nu} n_{\min}(x)$ and $\psi^{\rm fl}(n, \lambda \bar{R}) - \psi^{\rm st}(n, \lambda \bar{R}) > 0$ [see (27) and (32)]. Thus, one can prove (B7) if the following inequality holds:

$$\begin{aligned} &\frac{\partial}{\partial x} \int_{n_{\min}(x)}^{n_b(x)} \Phi(x) 2 \hat{P}(n) \psi^{\rm st}(n, \lambda \bar{R}) dn + \frac{\partial}{\partial x} \int_{n_b(x)}^{n_{\max}} \Phi(x) 2 \hat{P}(n) \psi^{\rm st}(n, \lambda \bar{R}) dn \leqslant 0 \Leftrightarrow \frac{\partial \Phi(x)}{\partial x} \int_{n_{\min}(x)}^{n_{\max}} 2 \hat{P}(n) \psi^{\rm st}(n, \lambda \bar{R}) dn \\ &- \Phi(x) \frac{\partial n_{\min}(x)}{\partial x} 2 \hat{P}[n_{\min}(x)] \psi^{\rm st}(n_{\min}(x), \lambda \bar{R}) \leqslant 0, \end{aligned} \tag{B8}$$

where

$$\frac{\partial \Phi(x)}{\partial x} = n_{\min}(x) \frac{\partial n_{\min}(x)}{\partial x} \Phi^2(x) \hat{P}[n_{\min}(x)] \Leftrightarrow n_{\min}(x) \int_{n_{\min}(x)}^{n_{\max}} \hat{P}(n) \psi^{\rm st}(n, \lambda \bar{R}) dn - \left[\int_{n_{\min}(x)}^{n_{\max}} \hat{P}(n) n dn \right] \psi^{\rm st}(n_{\min}(x), \lambda \bar{R}) \leqslant 0. \tag{B9}$$

The last inequality holds because the following conditions:

$$n_{\min}(x) \leqslant \int_{n_{\min}(x)}^{n_{\max}} \hat{P}(n) n dn, \text{ where } n_{\min}(x) \leqslant n \forall n \in \{n_{\min}(x), n_{\max}\}, \quad \int_{n_{\min}(x)}^{n_{\max}} \hat{P}(n) \psi^{\rm st}(n, \lambda \bar{R}) dn < \psi^{\rm st}(n_{\min}(x), \lambda \bar{R})$$

are satisfied in view of (1).

[1] J. Mandelkern, *Crystallization of Polymers* (McGraw–Hill, New York, 1964).
[2] K. H. Storks, J. Am. Chem. Soc. **60**, 1753 (1938).
[3] A. Keller, Philos. Mag. **2**, 1171 (1957).
[4] J. D. Hoffman and J. I. Lauritzen, Jr., J. Res. Natl. Bur. Stand., Sect. A **65A**, 297 (1961).
[5] P. J. Flory, J. Am. Chem. Soc. **84**, 2857 (1962).
[6] M. Dettenmaier, E. W. Fischer, and M. Starnrn, Polymer **9**, 343 (1980).
[7] D. Y. Yoon and P. J. Flory, Faraday Discuss. Chem. Soc. **68**, 288 (1979).
[8] D. G. H. Ballard, P. Cheshire, G. W. Longman, and J. Schelten, Polymer **19**, 379 (1978).
[9] J. Schelten, D. G. H. Ballard, G. D. Wignall, G. Longman, and W. Schmatz, Polymer **17**, 751 (1976).
[10] M. Negahban, Int. J. Solids Struct. **37**, 2777 (2000).
[11] I. J. Rao and K. R. Rajagopal, Z. Angew Math. Phys. **53**, 365 (2002).

[12] P. J. Flory, J. Chem. Phys. **15**, 397 (1947).
[13] P. J. Flory, J. Chem. Phys. **17**, 223 (1949).
[14] D. Göritz and F. H. Müller, Kolloid Z. Z. Polym. **251**, 679 (1973).
[15] D. Göritz and F. H. Müller, Kolloid Z. Z. Polym. **251**, 892 (1973).
[16] M. Saidan, Ph.D. thesis, Darmstadt Technische Universität, 2005.
[17] S. Ahzi, A. Makradi, R. V. Gregory, and D. D. Edie, Mech. Mater. **35**, 1139 (2003).
[18] R. B. Dupaix and D. Krishnan, Trans. ASME, J. Eng. Mater. Technol. **128**, 28 (2006).
[19] P. J. Flory, *Principles of Polymer Chemistry* (Cornell University Press, Ithaca, NY, 1971).
[20] J. Rault, J. Marchal, P. Judeinstein, and P. A. Albouy, Macromolecules **39**, 8356 (2006).
[21] Y. Fukahori, Polymer **51**, 1621 (2010).
[22] S. Toki, I. Sics, S. Ran, L. Liu, and B. Hsiao, Polymer **44**, 6003 (2003).
[23] S. Toki, I. Sics, B. Hsiao, S. Murakami, M. Tosaka, S. Poompradub, S. Kohjiya, and Y. Ikeda, J. Polymer Sci. Part B: Polymer Phys. **42**, 956 (2004).
[24] S. Toki, I. Sics, S. Ran, L. Liu, B. S. Hsiao, S. Murakami, K. Senoo, and S. Kohjiya, Macromolecules **35**, 6578 (2002).
[25] M. Tosaka, S. Murakami, S. Poompradub, S. Kohjiya, Y. Ikeda, S. Toki, I. Sics, and B. Hsiao, Macromolecules **37**, 3299 (2004).
[26] M. Kroon, Mech. Mater. **42**, 873 (2010).
[27] P. Zhang, G. Huang, L. Qu, Y. Nie, G. Weng, and J. Wu, J. Appl. Polym. Sci. **121**, 37 (2011).
[28] J. Carretero-Gonzalez, R. Verdejo, S. Toki, B. S. Hsiao, E. P. Giannelis, and M. A. López-manchado, Macromolecules **41**, 2295 (2008).
[29] G. Nie, Y.and Huang, L. Qu, X. Wang, G. Weng, and J. Wu, Polymer **52**, 3234 (2011).
[30] R. Dargazany and M. Itskov, Phys. Rev. E **88**, 012602 (2013).
[31] R. Dargazany, V. N. Khiêm, U. Navrath, and M. Itskov, J. Mech. Mater. Struct. **7**, 861 (2012).
[32] R. Dargazany, Ph.D. thesis, Faculty of Mechanical Engineering, RWTH Aachen University, 2011.
[33] R. Dargazany and M. Itskov, Int. J. Solids Struct. **46**, 2967 (2009).
[34] J. Chenal, C. Gauthier, L. Chazeau, L. Guy, and Y. Bomal, Polymer **48**, 6893 (2007).
[35] S. Poompradub, M. Tosaka, S. Kohjiya, Y. Ikeda, S. Toki, I. Sics, and B. S. Hsiao, J. Appl. Phys. **97**, 103529 (2005).
[36] M. Itskov, R. Dargazany, and K. Hörnes, Math. Mech. Solids **17**, 693 (2012).
[37] M. Puso, Ph.D. thesis, University of California, Davis, 2003.
[38] S. Govindjee and J. Simo, J. Mech. Phys. Solids **39**, 87 (1991).
[39] S. Göktepe and C. Miehe, J. Mech. Phys. Solids **53**, 2259 (2005).
[40] Y. Merckel, M. Brieu, J. Diani, and J. Caillard, J. Mech. Phys. Solids **60**, 1257 (2012).
[41] G. Machado, G. Chagnon, and D. Favier, Mech. Mater. **50**, 70 (2012).
[42] F. Bueche, J. Appl. Polym. Sci. **5**, 271 (1961).
[43] S. Govindjee, Rubber Chem. Technol. **70**, 25 (1997).
[44] J. Bergström and M. Boyce, Rubber Chem. Technol. **72**, 633 (1999).
[45] B. Huneau, Rubber Chem. Technol. **84**, 425 (2011).
[46] S. Murakami, K. Senoo, S. Toki, and S. Kohjiya, Polymer **43**, 2117 (2002).
[47] E. H. Andrews, Pure Appl. Chem. **31**, 91 (1972).
[48] E. A. Poshtan, R. Dargazany, and M. Itskov, in *Constitutive Models for Rubber VII* (Taylor & Francis Group, London, UK, 2011), p. 215.
[49] R. Dargazany, V. N. Khiêm, and M. Itskov, International Journal of Plasticity (2014), doi:10.1016/j.ijplas.2013.12.004
[50] M. Tosaka, Polymer J. **39**, 1207 (2007).
[51] S. Trabelsi, P. Albouy, and J. Rault, Macromolecules **36**, 7624 (2003).
[52] V. N. Khiêm, R. Dargazany, and M. Itskov, in *Constitutive Models for Rubber VIII* (Taylor & Francis Group, London, UK, 2013), p. 253.
[53] S. D. Gehman and J. E. Field, J. Appl. Phys. **10**, 564 (1939).
[54] S. Toki, I. Sics, S. Ran, L. Liu, B. S. Hsiao, S. Murakami, M. Tosaka, S. Kohjiya, S. Poompradub, Y. Ikeda, and A. H. Tsou, Rubber Chem. Technol. **77**, 317 (2004).
[55] S. Heo and Y. Xu, Math. Comput. **70**, 269 (2000).
[56] A. E. Ehret, M. Itskov, and H. Schmid, Int. J. Numer. Methods Eng. **81**, 189 (2010).
[57] J.-B. Le Cam, Rubber Chem. Technol. **83**, 247 (2010).
[58] H. M. James and E. Guth, J. Chem. Phys. **11**, 455 (1943).
[59] A. D. Drozdov, Int. J. Non-Linear Mech. **34**, 807 (1999).
[60] I. J. Rao and K. R. Rajagopal, Int. J. Solids Struct. **38**, 1149 (2001).
[61] M. Itskov, *Tensor Algebra and Tensor Analysis for Engineers* (Springer, Berlin, 2012).